Nano Research

Open Access

Research Article

Growth modes of β-Ga_2O_3 on h-BN: Remote epitaxy and van der Waals epitaxy

Yiming Shi[1,2], Junhua Meng[1] ✉, Zhengchang Xia[2,3], Jidong Huang[2,3], Wenkang Liu[1], Ji Jiang[2,3], Zhigang Yin[2,3], Jinxiang Deng[1], and Xingwang Zhang[2,3] ✉

[1] *School of Physics and Optoelectronic Engineering, Beijing University of Technology, Beijing 100124, China*
[2] *Key Lab of Semiconductor Materials Science, Institute of Semiconductors, Chinese Academy of Sciences, Beijing 100083, China*
[3] *Center of Materials Science and Optoelectronics Engineering, University of Chinese Academy of Sciences, Beijing 100049, China*

Cite this article: *Nano Research*, **2025**, *18*, 94907129. https://doi.org/10.26599/NR.2025.94907129

ABSTRACT: Integrating monoclinic gallium oxide (β-Ga_2O_3) with two-dimensional (2D) hexagonal boron nitride (h-BN) into heterostructures is of significant importance for achieving high-power device applications. The 2D-material-assisted epitaxy provides a straightforward integration method for fabricating β-Ga_2O_3/h-BN vertical heterostructures. In this work, the β-Ga_2O_3 films were deposited on both polycrystalline and single-crystalline h-BN layers with different thicknesses, and two growth modes of β-Ga_2O_3 films on h-BN, remote epitaxy, and van der Waals (vdW) epitaxy, were investigated. The results show that the potential of the sapphire substrate can penetrate the monolayer and bilayer h-BN to obtain the remote epitaxy of β-Ga_2O_3 films, regardless of the crystallinity of h-BN. The vdW epitaxy of β-Ga_2O_3 film can be realized on the monocrystalline h-BN substrate. Compared with the conventional and remote epitaxial β-Ga_2O_3 films on sapphire substrate, the vdW epitaxial β-Ga_2O_3 films on the single-crystalline h-BN substrate exhibit higher crystallinity. This work indicates that the 2D-material-assisted epitaxy provides a feasible scheme for the heterogeneous integration of β-Ga_2O_3 films.

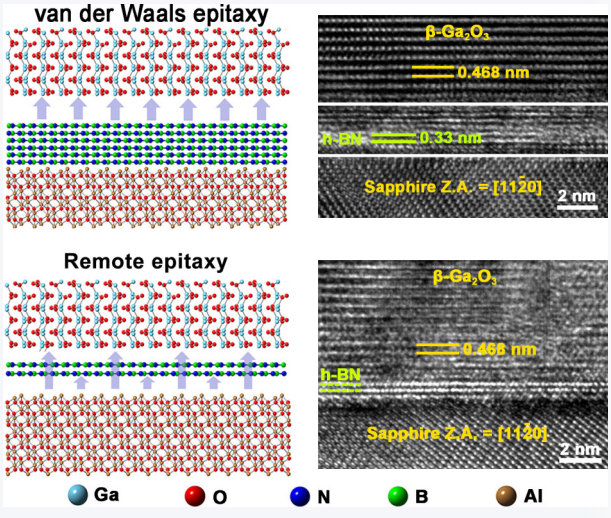

KEYWORDS: β-Ga_2O_3, h-BN, remote epitaxy, van der Waals epitaxy, heterostructures

1 Introduction

As an emerging ultra-wide bandgap semiconductor, monoclinic gallium oxide (β-Ga_2O_3) has shown great development potential in the fields of high-power high-frequency electronic devices due to its outstanding properties such as high breakdown electric field, excellent thermal stability, and large Baliga's figure of merit. However, the downside of β-Ga_2O_3 is that it has a relatively low thermal conductivity (0.11–0.27 W/(cm·K)), which poses an urgent challenge for heat dissipation of power devices and thus prevents the development of β-Ga_2O_3-based power devices [1–4]. One promising direction for addressing this problem is to realize heterogeneous integration of β-Ga_2O_3 with high thermal conductivity substrates. Recently, the direct growth of β-Ga_2O_3 on highly thermally conductive diamond [5, 6], SiC [7], and GaN [8] has been demonstrated. Nevertheless, the lattice matching constraints in conventional heteroepitaxy have greatly narrowed down the choices of available substrates. Another alternative approach for heterogeneous integration is to transfer the β-Ga_2O_3 films onto high thermal conductivity substrates. For example, the β-Ga_2O_3-based devices exhibited a significantly improved thermal stability by transferring β-Ga_2O_3 to highly thermally conductive SiC substrates via ion cutting technique [9, 10].

Recent emerging two-dimensional (2D)-material-assisted epitaxy techniques, including remote epitaxy and van der Waals (vdW) epitaxy, have shown exciting perspectives due to many potential advantages, such as elimination of the lattice matching constraints, and easy exfoliation and transfer. Remote epitaxy is a process that the substrate and the epilayer have remote interaction, in which the

Received: September 1, 2024; **Revised:** October 3, 2024
Accepted: November 13, 2024

✉Address correspondence to Junhua Meng, jhmeng@bjut.edu.cn; Xingwang Zhang, xwzhang@semi.ac.cn

electrostatic potential of substrate is not completely shielded by the 2D interlayer and the epilayer follows the crystalline template of substrate [11–13]. In contrast, directly growing three-dimensional (3D) materials on the surface of 2D materials, wherein the substrate and the epitaxial layer are combined by van der Waals forces, is called as vdW epitaxy [11, 14]. Up to now, the 2D-material-assisted epitaxy has been primarily focused on nitride semiconductors such as GaN and AlN [15–19], only a few studies focused on the 2D-material-assisted growth of Ga_2O_3 films with graphene [20–22]. Unfortunately, the graphene is very susceptible and can be severely damaged in harsh growth environments such as plasma, oxidation, and high-temperature [23, 24]. Contrarily, wide bandgap hexagonal boron nitride (h-BN), a structural analogue of graphene, possesses extremely high chemical and thermal stability [25] and it is also regarded as a promising interlayer for the 2D-material-assisted epitaxy [11, 26]. Furthermore, high thermal conductivity of h-BN together with excellent dielectric and insulation properties makes it ideal for integrating β-Ga_2O_3 with h-BN. In recent years, the 2D-material-assisted epitaxy using h-BN as interlayer has been reported for the growth of nitrides and sulfides [11, 26–28]. Nevertheless, there has never been any report on the growth of β-Ga_2O_3 film on 2D h-BN interlayer. On the other hand, although both remote epitaxy and vdW epitaxy have been reported in many previous studies [14, 29, 30], there is a lack of growth mechanism capable of clearly distinguishing the remote epitaxy and the vdW epitaxy, especially for the 2D-material-assisted epitaxy using h-BN. According to the principles of two growth modes, the investigation on the effect of the features of the h-BN layers on the growth of β-Ga_2O_3 films can provide an insight into the growth mechanism of two epitaxy modes.

In this work, the β-Ga_2O_3 thin films were epitaxially grown on 2D h-BN layers for the first time, and the determination of the preferred epitaxy for β-Ga_2O_3 on 2D h-BN interlayers with different thicknesses and crystallinities was investigated. Here, two kinds of h-BN template (polycrystalline and single-crystalline h-BN layers) are chosen to unveil the impact of crystallinity of h-BN interlayer on the epitaxial interaction, and sapphire is used as substrate because its high ionicity of 0.594 [15] provides a strong interfacial interaction for the remote epitaxy. In this case, it is found that the potential of the sapphire substrate can penetrate the monolayer and bilayer h-BN to achieve the remote epitaxy of β-Ga_2O_3 thin films, regardless of the crystallinity of h-BN. The vdW epitaxy results in a high-quality single-crystalline β-Ga_2O_3 thin film with an epitaxial relationship of β-Ga_2O_3 $(\bar{2}01)[010]||$h-BN $(0001)[1\bar{1}00]||$sapphire $(0001)[1\bar{1}00]$. The results show that the remote epitaxy is mainly affected by the number of h-BN layers, and the vdW epitaxial β-Ga_2O_3 films on the thicker single-crystalline h-BN substrate exhibit higher crystallinity.

2 Results and discussion

Many studies have successfully demonstrated the feasibility of remote epitaxy of 3D materials on h-BN [14, 29, 30]. However, the research of remote epitaxy of β-Ga_2O_3 on h-BN is still lacking. In order to assess the feasibility of remote epitaxy of β-Ga_2O_3, density functional theory (DFT) was used to calculate the remote interaction between Al-terminated c-sapphire and β-Ga_2O_3. Here, periodic boundary conditions were imposed along the dashed lines of simulation model (Fig. 1(a)). As shown in Figs. 1(b) and 1(c), there is a significant charge density overlap between the separated sapphire and β-Ga_2O_3 slabs within a gap of about 7 Å (corresponding to a gap of bilayer h-BN). To distinctly display the evolution of the charge density with the interaction gap, Figs. 1(d)–1(g) and Fig. S1 in the Electronic Supplementary Material (ESM) respectively show the charge density distribution of the Al- and O-terminated c-sapphire surface, as well as through different interaction gaps that are equivalent to the thicknesses of monolayer, bilayer, and tri-layer h-BN. As shown in Figs. 1(d)–1(f) and Fig. S1(a)–S1(c) in the ESM, the penetration of the potential fluctuation in sapphire through monolayer and bilayer h-BN is clearly visible and thus the pattern of potential distribution is well remained. Nevertheless, the potential fluctuation is seriously dampened when

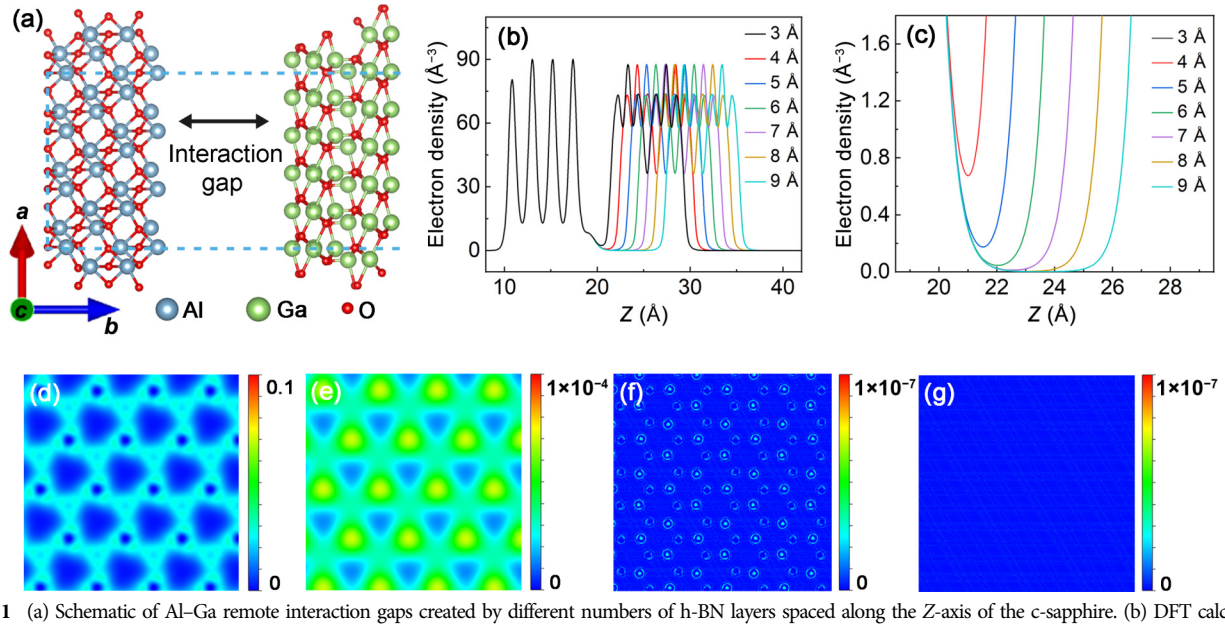

Figure 1 (a) Schematic of Al–Ga remote interaction gaps created by different numbers of h-BN layers spaced along the *Z*-axis of the c-sapphire. (b) DFT calculating electron density along separated slabs of Al-terminated c-sapphire and β-Ga_2O_3. (c) An enlarged view of the electron density within the gap region in (b). Charge density distribution of the Al-terminated c-sapphire through different interaction gaps equivalent to different numbers of h-BN layers: (d) without h-BN interlayer, (e) monolayer h-BN, (f) bilayer h-BN, and (g) tri-layer h-BN.

the interaction gap increases to tri-layer h-BN (Fig. 1(g) and Fig. S1(d) in the ESM). These theoretically calculated results indicate that the potential field of sapphire substrate can penetrate the monolayer and bilayer h-BN, and the influence of sapphire can be completely shielded when the gap is increased beyond bilayer h-BN.

To reveal the effect of crystallinity of h-BN interlayer on the epitaxial interaction, both polycrystalline and single-crystalline h-BN layers were used to serve as interlayers for the 2D-material-assisted epitaxy. Polycrystalline h-BN templates with different layers were grown on Cu foils by ion beam sputtering deposition (IBSD) technique [31]. Figures 2(a)–2(c) show the scanning electron microscopy (SEM) images of monolayer, bilayer, and tri-layer h-BN grown on Cu foils for different time. Except for the faint grain boundaries and a few wrinkles, the monolayer h-BN shows rather uniform contrast overall (Fig. 2(a)), indicating good continuity and thickness uniformity. As the number of h-BN layers increases, the secondary nucleation at grain boundaries becomes more pronounced (Figs. 2(b) and 2(c)). To enable the remote epitaxy of β-Ga_2O_3, the h-BN layers on Cu foils were transferred onto sapphire substrates by the wet-etching transfer method. Figure 2(d) and Fig. S2 in the ESM show the atomic force microscopy (AFM) images of transferred h-BN layers, which exhibit a similar morphology to those of the as-grown h-BN layers. The X-ray photoelectron spectroscopy (XPS) full-survey spectrum (Fig. S3 in the ESM) reveals that the transferred h-BN layer is of high chemical purity, except for the C contamination from adsorption of hydrocarbons due to sample transport in air. The XPS B 1s and N 1s core levels of monolayer h-BN are located at 190.7 and 398.1 eV, respectively (Fig. 2(e)) [32, 33]. The atomic ratio of B and N calculated from the XPS peak intensities and their sensitivity factors is 1.00:1.02, close to the stoichiometry of h-BN, revealing that the transfer process did not degrade the quality of h-BN layer. To evaluate the thickness and crystallinity of h-BN layers, the Raman spectra of the transferred h-BN with different layers were measured. As shown in Fig. 2(f), all the h-BN layers exhibit a clear and sharp E_{2g} mode at 1365 cm^{-1}, in which the peak intensity of E_{2g} mode is roughly proportional to the number of layers of h-BN. The peak widths of the E_{2g} mode (full-width at half-maximum (FWHM)) for the monolayer, bilayer, and tri-layer h-BN are 19.8, 17.5, and 17.4 cm^{-1}, respectively, indicating that the crystallinity of h-BN is almost independent of its number of layers.

To validate theoretical prediction, the β-Ga_2O_3 films were grown by low-pressure chemical vapor deposition (LPCVD) at 800 °C on sapphire substrates with various thicknesses of the transferred polycrystalline h-BN interlayer. The thickness of the β-Ga_2O_3 film is about 250 nm (Fig. S4 in the ESM). Figure 3(a) shows Raman spectra of the β-Ga_2O_3 films grown on sapphire with and without h-BN interlayers, and six Raman-active modes (marked by #) are clearly observed for all the β-Ga_2O_3 films. The low frequency modes at 169.2 and 200.1 cm^{-1} are attributed to the vibration and translation of tetrahedra–octahedra chains, respectively [34], while the mid frequency peaks at 320.1, 346.5, and 474.9 cm^{-1} are associated with the deformation of Ga_2O_6 octahedra [35], and the high frequency mode at 654.9 cm^{-1} is assigned to the bending vibration of GaO_4 tetrahedra [36]. These Raman peaks are well consistent with the previously reported values of β-Ga_2O_3 [37, 38]. Moreover, the E_{2g} mode of monolayer h-BN at 1367 cm^{-1} remains almost unchanged after the β-Ga_2O_3 growth (Fig. S5 in the ESM), manifesting that the chemical vapor deposition (CVD) growth of β-Ga_2O_3 has almost no effect even for the monolayer h-BN.

Figure 3(b) shows the X-ray diffraction (XRD) θ–2θ patterns of the β-Ga_2O_3 films grown on sapphire with and without h-BN layer. For the β-Ga_2O_3 films on sapphire with monolayer and bilayer h-BN, besides the peaks from sapphire substrate, only three peaks corresponding to the monoclinic β-Ga_2O_3 ($\bar{2}01$), ($\bar{4}02$), and ($\bar{6}03$) planes are clearly observed at 18.99°, 38.34°, and 59.12°, respectively, suggesting a high ($\bar{2}01$) orientation of the β-Ga_2O_3 layers. The β-

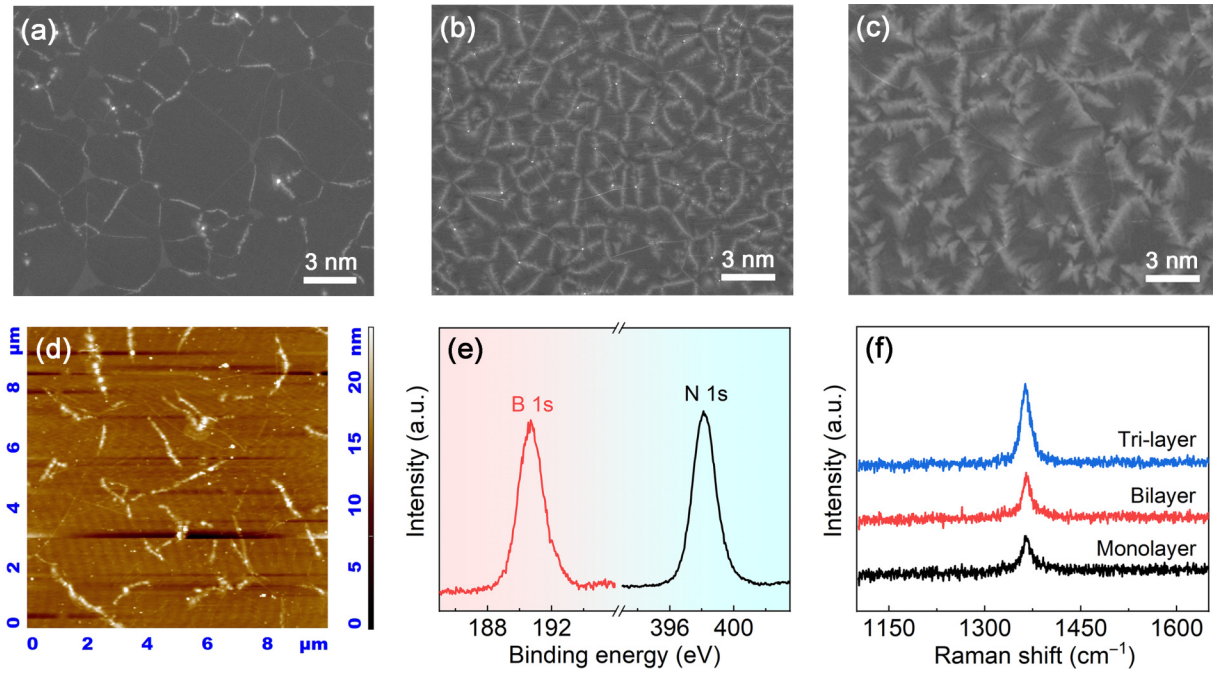

Figure 2 Typical SEM images of IBSD-grown (a) monolayer, (b) bilayer, and (c) tri-layer polycrystalline h-BN on Cu foils. (d) AFM image of the monolayer h-BN transferred onto a sapphire substrate. (e) XPS spectra of B 1s and N 1s core levels of the polycrystalline h-BN. (f) Raman spectra of the polycrystalline h-BN with different layer numbers transferred onto sapphire substrates.

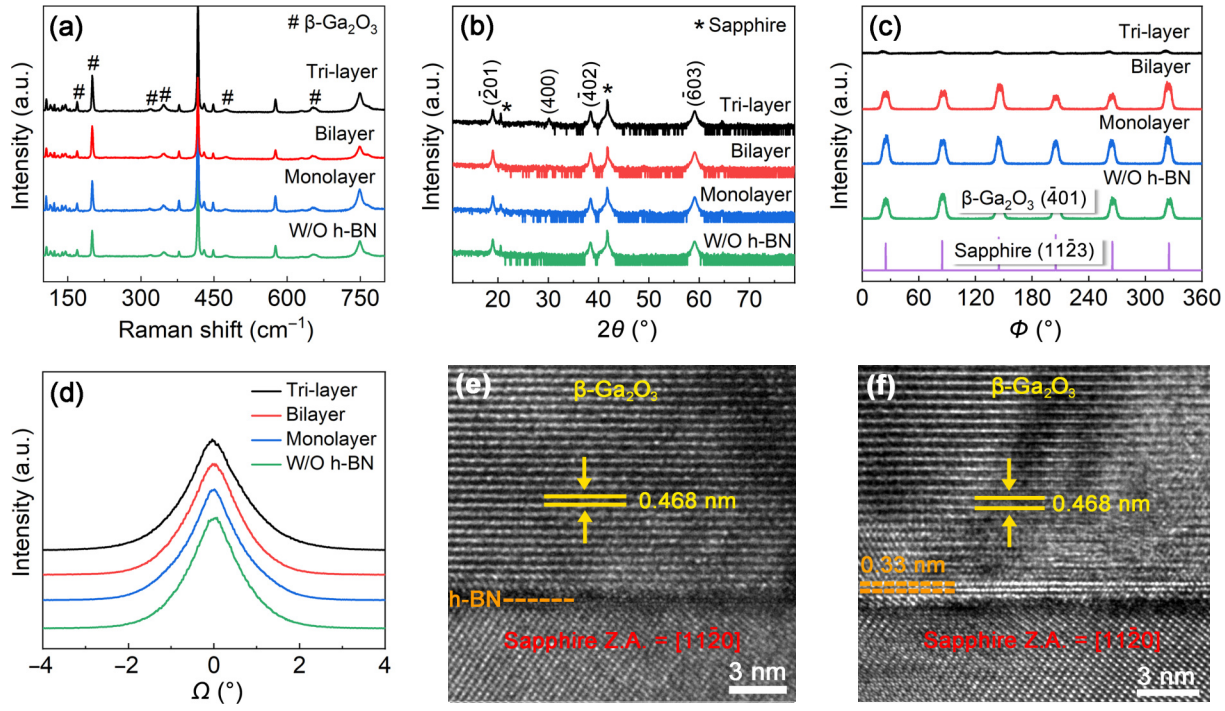

Figure 3 (a) Raman spectra, (b) XRD θ–2θ patterns, (c) Φ-scan patterns, and (d) rocking curves of ($\bar{2}01$) plane of the β-Ga_2O_3 thin films grown on sapphire with and without polycrystalline h-BN interlayers. (e) Cross-sectional HRTEM images of the β-Ga_2O_3 thin films on sapphire through (e) monolayer and (f) bilayer polycrystalline h-BN.

Ga_2O_3 film directly grown on sapphire without h-BN shows the similar XRD pattern. However, for the β-Ga_2O_3 film on a tri-layer h-BN, an additional diffraction peak at 30.12° corresponding to the β-Ga_2O_3 (400) reflection appears, implying that it is polycrystalline structure.

To disclose the orientational relationship between the β-Ga_2O_3 film and sapphire substrate, the in-plane orientation of the β-Ga_2O_3 epilayer was further characterized by XRD Φ-scan on the β-Ga_2O_3 ($\bar{4}01$) and sapphire ($11\bar{2}3$) reflections, as shown in Fig. 3(c). Similar to the θ–2θ patterns, all the XRD Φ-scan patterns are similar for the β-Ga_2O_3 films without and with monolayer and bilayer h-BN. Six peaks with an interval of 60° are observed for the β-Ga_2O_3 ($\bar{4}01$) reflection, which accurately coincide with the positions of sapphire ($11\bar{2}3$) reflection. Since monoclinic β-Ga_2O_3 has only a twofold symmetry along <010> [39–41], and thus the six peaks of the β-Ga_2O_3 ($\bar{4}01$) observed in Fig. 3(c) manifest that there are three equivalent domains involved in these β-Ga_2O_3 films. Combining the XRD θ–2θ scans, the epitaxial relation between the β-Ga_2O_3 films and the sapphire substrate can be deduced as β-Ga_2O_3 ($\bar{2}01$)[010]//sapphire (0001)[$1\bar{1}00$]. The corresponding epitaxial relationship is the same as that of the direct growth of β-Ga_2O_3 on sapphire (0001) substrates [40]. Interestingly, when a tri-layer h-BN is introduced between β-Ga_2O_3 and sapphire, the intensity of β-Ga_2O_3 ($\bar{4}01$) reflection is significantly reduced to almost disappear, revealing the loss of the in-plane epitaxial relationship. The experimental results are entirely consistent with the above DFT calculations, which predict that the potential field of substrate is nearly completely screened by the tri-layer h-BN and thus cannot guide the remote epitaxy of β-Ga_2O_3. To evaluate the effect of h-BN interlayer on the crystalline quality of the β-Ga_2O_3 epilayer, the XRD rocking curves (XRC, Ω-scans) of β-Ga_2O_3 ($\bar{2}01$) reflection were measured. As shown in Fig. 3(d), the XRC-FWHM values of the β-Ga_2O_3 films without and with monolayer h-BN are found to be almost the identical (1.31° and 1.32°), while they respectively increase to 1.39° and 1.48° when introducing the bilayer and tri-layer h-BN. Obviously, the monolayer h-BN does not affect the out-of-plane alignment of the remote epitaxial β-Ga_2O_3 film. However, the crystallinity of the epilayer is slightly degraded with increasing the number of h-BN layers, which is also supported by the variation of the FWHM of the β-Ga_2O_3 Raman peak (Fig. S6 in the ESM).

The crystalline quality and interfacial structure of the β-Ga_2O_3 grown on sapphire with monolayer and bilayer h-BN were further investigated by cross-sectional high-resolution transmission electron microscopy (HRTEM). As shown in Figs. 3(e) and 3(f), the lattice fringes of 0.468 nm, as marked by the yellow parallel lines, match well with the d-space of the β-Ga_2O_3 ($\bar{2}01$) planes, indicating that the ($\bar{2}01$) planes of β-Ga_2O_3 film are parallel to the c-planes of sapphire substrate. The presence of monolayer and bilayer h-BN is clearly visible between the β-Ga_2O_3 epilayer and sapphire substrate with atomically sharp interface. It is clear that the introduction of monolayer and bilayer h-BN has almost no effect on the epitaxial growth of β-Ga_2O_3 on sapphire. The HRTEM and XRD results are very consistent with the above DFT calculations, which predict that the potential field of sapphire substrate is rapidly decayed with the increased epilayer–substrate gap and the remote epitaxy of β-Ga_2O_3 on sapphire is possible within a 7 Å gap.

To explore the effect of h-BN crystallinity on the 2D-material-assisted epitaxy, the single-crystalline h-BN layers with controllable thicknesses from monolayer to tens of nanometers were also synthesized on sapphire substrates by submicron-spacing vapor deposition (SSVD) method [42]. Herein, the thickness of h-BN layers was controlled by varying the growth time of boron film that was used as the B source during the SSVD growth. Figure S7 in the ESM shows the Raman spectra of the h-BN layers synthesized from the boron films with different growth time from 5 to 50 min. The Raman intensity increases with the growth time of boron film,

verifying that the thickness of h-BN layer can be indeed controlled by the growth time of boron film. In particular, the SSVD-grown h-BN layer exhibits an extremely narrow Raman peak whose FWHM is as narrow as 10 cm^{-1} (Fig. 4(a)) and comparable to those of bulk single-crystal h-BN (9 cm^{-1}) [43]. The Raman results indicate that the SSVD-grown h-BN layers possess extremely high crystallinity, which is also confirmed by transmission electron microscopy (TEM) measurements. Figure 4(b) shows the cross-sectional HRTEM image of the SSVD-grown h-BN layer taken along the zone axis of c-sapphire [1$\bar{1}$00]. The 15-min boron film leads to the formation of 7-layers of h-BN, and the well-defined and continuous layered structure certificates high crystalline quality. The interlayer distance of 0.33 nm is consistent with that of basal plane of bulk h-BN. The lateral lattice spacing of h-BN is measured to be 0.25 nm, which matches well with the lattice spacing of h-BN [11$\bar{2}$0] (i.e., zigzag direction of h-BN). Consequently, the epitaxial relationship between the h-BN epilayer and the sapphire substrate can be concluded as h-BN (0001)[11$\bar{2}$0]||sapphire (0001)[11$\bar{2}$0], as schematically illustrated in Fig. 4(c). Because of the mismatch in thermal expansion coefficient between h-BN and sapphire [42, 44], a network of wrinkles is observed on the continuous and homogeneous h-BN surface (Fig. 4(d) and Fig. S8 in the ESM). The layer number of h-BN is still maintained throughout the wrinkle, indicating the uniformity and continuity of 2D h-BN even in the presence of wrinkles [42]. Furthermore, the extremely high growth temperature of h-BN leads to the formation of atomic step-terrace structure from sapphire substrate.

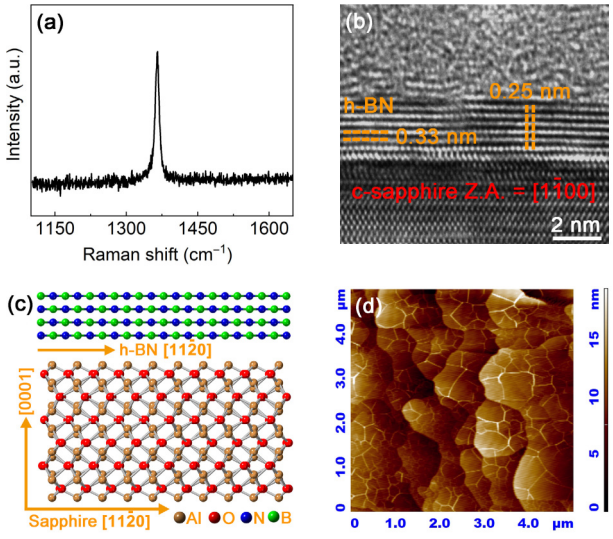

Figure 4 (a) Raman spectrum of the SSVD-grown single-crystalline h-BN on sapphire. (b) Cross-sectional HRTEM image of the SSVD-grown single crystal h-BN on sapphire. (c) Sectional view of the schematic drawing of the epitaxial relationship between h-BN and sapphire. (d) Typical AFM image of the SSVD-grown single crystal h-BN on sapphire.

Finally, the β-Ga_2O_3 was also grown on the single-crystalline h-BN layers with different thicknesses. As expected, when the β-Ga_2O_3 thin film was grown on the sapphire covered by a single-crystalline monolayer h-BN, the remote epitaxy of β-Ga_2O_3 on sapphire can be realized through monolayer h-BN, with a slight narrow XRC-FWHM of 1.28° (Fig. S9 in the ESM). Apparently, the potential of the sapphire substrate can penetrate the monolayer h-BN to obtain the remote epitaxy of β-Ga_2O_3 films, regardless of the crystallinity of h-BN. In contrast, the crystallinity of h-BN has a determinant effect on the growth of β-Ga_2O_3 on the thick h-BN layers. Figure 5(a) shows the XRD θ–2θ pattern of the β-Ga_2O_3 films grown on the 2.0 and 7.3 nm single-crystalline h-BN/sapphire substrates. Besides the diffraction peaks from h-BN interlayer and sapphire substrate, only the diffraction peaks from β-Ga_2O_3 ($\bar{2}$01), ($\bar{4}$02), and ($\bar{6}$03) planes are observed. Their XRD Φ-scan patterns are similar to those of the remote epitaxial β-Ga_2O_3 films grown on sapphire through monolayer or bilayer h-BN, where six peaks of β-Ga_2O_3 ($\bar{4}$01) reflection are clearly presented and their peak positions are identical with those of sapphire (11$\bar{2}$3) reflections (Fig. 5(b)). Clearly, the identical epitaxial relationship between the β-Ga_2O_3 films and the single-crystalline h-BN with thicknesses of 2.0 and 7.3 nm is achieved as the remote epitaxy: β-Ga_2O_3 ($\bar{2}$01)[010]//sapphire (0001)[1$\bar{1}$00]. Since the thickness of h-BN is far exceeds the largest remote interaction distance of 7 Å, we propose that the vdW epitaxy is responsible for such results. Generally, the flat surface of 2D h-BN lacks dangling bonds, which makes it difficult to form nucleation sites for the vdW epitaxy. Herein, a large number of wrinkles naturally formed during the growth of h-BN can serve as nucleation sites. It is well known that the single crystal structure of h-BN substrate is necessary for the vdW epitaxy. Indeed, we find that the in-plane orientation of the β-Ga_2O_3 film on a 2.0 nm thick polycrystalline h-BN is completely random (Fig. S10 in the ESM), which provides an additional proof for the vdW epitaxy through single-crystalline h-BN. Furthermore, the XRC-FWHM values of the β-Ga_2O_3 films grown on the 2.0 and 7.3 nm h-BN are 0.98° and 0.89°, respectively (Fig. 5(c)), when the 200.1 cm^{-1} Raman mode exhibits the nearly same FWHM (2.8 and 2.7 cm^{-1} for the 2.0 and 7.3 nm samples, respectively, Fig. S11 in the ESM). Both FWHM values are much narrower than those of the remote epitaxial and conventional epitaxial counterparts [45, 46], demonstrating the potential advantages of vdW epitaxy in terms of crystallinity of epilayer. In addition, the XPS survey spectrum shows that the β-Ga_2O_3/h-BN film is of high chemical purity with negligible impurities (Fig. S12 in the ESM). The XPS core level spectra of Ga 2p and O 1s are displayed in Fig. 5(d). The peaks located at 530.5, 1117.5, and 1144.4 eV correspond to O 1s, Ga $2p_{3/2}$, and Ga $2p_{1/2}$, respectively, which is in good agreement with the previous reports [47, 48].

The cross-sectional HRTEM images and energy dispersive X-ray spectroscopy (EDS) element mapping were performed to investigate the microstructure of the vdW epitaxial β-Ga_2O_3 film. As shown in Figs. 5(e) and 5(f), the perfectly uniform and sharp interfaces are formed between the β-Ga_2O_3 epilayer, the single-crystalline h-BN, and the sapphire substrate. For all the samples with different thicknesses of h-BN layers, both the epitaxial β-Ga_2O_3 and the h-BN interlayer show excellent layered structure with no obvious defects (Figs. 5(f) and 5(g), and Fig. S13 in the ESM). The HRTEM images (Figs. 5(f) and 5(g)), which were taken along the zone axis of sapphire [11$\bar{2}$0] direction, show that the β-Ga_2O_3 ($\bar{2}$01) plane is parallel to the basal plane of h-BN and the sapphire (0001) plane. Moreover, the in-plane orientation relationship between the epilayer and h-BN can be determined by measuring their lateral lattice spacing. As shown in Fig. 5(g), the lateral lattice spacings of β-Ga_2O_3 and h-BN are 0.30 and 0.22 nm, respectively. The former is well consistent with the lattice spacing of the β-Ga_2O_3 [010] direction, and the latter matches well with the lattice spacing of h-BN [1$\bar{1}$00] direction. Combining these results, the epitaxial relationship of β-Ga_2O_3/h-BN/sapphire system can be determined as β-Ga_2O_3 ($\bar{2}$01)[010]//h-BN (0001)[1$\bar{1}$00]//sapphire (0001)[1$\bar{1}$00], which is further confirmed by the selected area electron diffraction (SAED) pattern of HRTEM image, as shown in Fig. 5(h).

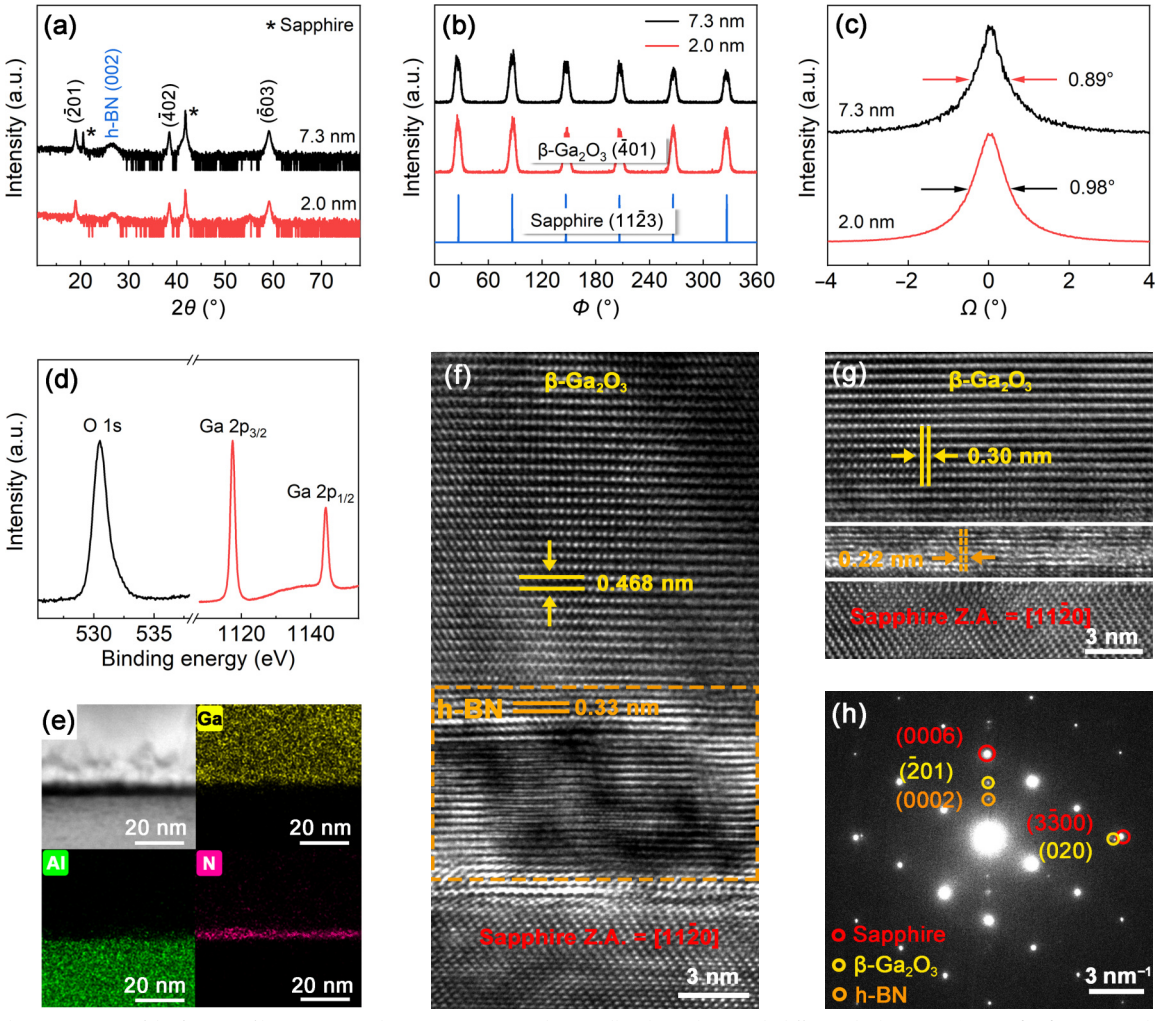

Figure 5 Characterization of the β-Ga_2O_3 films grown on the SSVD-grown single-crystalline h-BN layer with different thicknesses. (a) XRD θ–2θ pattern and (b) XRD Φ-scan pattern for the β-Ga_2O_3 ($\bar{4}01$) and sapphire ($11\bar{2}3$) reflections. (c) XRD rocking curves of β-Ga_2O_3 ($\bar{2}01$) reflection. (d) XPS core level spectra of O 1s and Ga 2p. (e) EDS element mappings of Ga, Al, and N atoms for the β-Ga_2O_3/h-BN/sapphire heterointerface. Cross-sectional HRTEM images of the β-Ga_2O_3 films grown on (f) 7.3 nm and (g) 2.0 nm single-crystalline h-BN. (h) SAED pattern of HRTEM image taken from the interface area in (f).

It is clear that both remote epitaxy and vdW epitaxy of β-Ga_2O_3 have been demonstrated by adopting the 2D h-BN layers with different thicknesses and crystallinities. The potential field of sapphire substrate can penetrate the monolayer and bilayer h-BN to achieve the remote epitaxy of β-Ga_2O_3, while their epitaxial relationship is gradually deteriorated with increasing h-BN layer number. Since the lattice orientation is imprinted by the sapphire substrate for the remote epitaxy, the crystallinity of h-BN interlayer has no obvious effect during the remote epitaxy of β-Ga_2O_3. In contrast, the vdW epitaxy of β-Ga_2O_3 can only be achieved on the single-crystalline h-BN substrate, in which the lattice orientation of epilayer is determined by the lattice symmetry of h-BN and the strict requirement on lattice matching for the conventional epitaxy is not necessary.

3 Conclusions

In summary, the β-Ga_2O_3 films were grown on polycrystalline and single-crystalline h-BN layers with different thicknesses. Theoretical and experimental results indicate that the potential field of sapphire substrate is rapidly decayed within a 7 Å gap, and thus the remote epitaxy of β-Ga_2O_3 on sapphire can be realized through monolayer and bilayer h-BN. The crystalline quality of the remote epitaxial β-Ga_2O_3 films is degraded with increasing h-BN thickness, while the crystallization characteristics of the h-BN interlayer has almost no effect on the quality of epilayer. The vdW epitaxy of β-Ga_2O_3 film can only be achieved on the single-crystalline h-BN substrate, and their epitaxial relationship can be determined as β-Ga_2O_3 ($\bar{2}01$)[010]||h-BN (0001)[$1\bar{1}00$]||sapphire (0001)[$1\bar{1}00$]. Compared with the conventional and remote epitaxial β-Ga_2O_3 films on sapphire substrates, the vdW epitaxial β-Ga_2O_3 film on the single-crystalline h-BN substrate exhibits higher crystallinity, which is attributed to the lattice guidance-capable vdW interaction between β-Ga_2O_3 and h-BN. This work proves the feasibility of growing β-Ga_2O_3 films by the remote epitaxy and vdW epitaxy using h-BN interlayer, which provides a new scheme for the heterogeneous integration of β-Ga_2O_3 films.

4 Experimental

4.1 Synthesis and transfer of polycrystalline h-BN

The polycrystalline h-BN layers with different thicknesses were synthesized on Cu foils by IBSD. Prior to the growth, the Cu foils

were sequentially cleaned with acetone, isopropanol, and ethanol, and then the surface oxide layer was removed with a dilute nitric acid solution. The h-BN layers were deposited on the cleaned Cu foils at a substrate temperature of 1050 °C and a pressure of 3.5×10^{-2} Pa by sputtering h-BN target with a 1 keV Ar ion beam. The number of h-BN layer was controlled by varying the growth time. The IBSD-grown h-BN layers were transferred onto sapphire substrates by the wet-transfer method. Firstly, the rosin solution was spin-coated on the h-BN/Cu and condensed at room temperature to form a support layer. After that, the copper foil was dissolved in $FeCl_3$ etchant until it was completely etched. Subsequently, the $FeCl_3$ solution was diluted with deionized water and the rosin/h-BN was transferred to the sapphire substrate. Then, the rosin layer was dissolved in acetone, isopropanol, and ethanol in sequence. At last, the h-BN/sapphire was annealed in air at 700 °C for 30 min.

4.2 Preparation of single-crystalline h-BN layers

The single-crystalline h-BN layers were grown on c-sapphire substrates by SSVD method, which was detailly depicted in our previous study [42]. The B films were deposited on the sapphire substrate by pulsed laser deposition with a 248 nm KrF laser at a repetition rate of 5 Hz and pulse laser energy of 500 mJ, in which the substrate temperature was kept at 1100 °C and the growth time was varied from 5 to 50 min. Then, the B film that was used as B solid source was covered face-to-face by the sapphire substrate and it was placed in a tube furnace. N_2 gas was introduced into the chamber and the pressure was maintained at 1.5 atm. When the temperature was raised to 1700 °C, the B atoms were sublimated and reacted with N_2 to form h-BN layer on the covered sapphire. The growth time was maintained for 30 min. Finally, the tube furnace was cooled to room temperature in N_2 atmosphere after the growth.

4.3 Preparation of β-Ga_2O_3 thin films

The β-Ga_2O_3 thin films were grown on the h-BN/sapphire substrates by LPCVD, which consisted of a two-inch tubular quartz reactor and two independently controlled temperature zones. High-purity Ga pellets and O_2 served as precursors, and Ar gas was used as the carrier gas. Ga pellets were placed in a quartz boat upstream of the quartz tube reactor, while h-BN/sapphire substrates were placed at the downstream about 35 cm away from the Ga source. The quartz tube was firstly pumped to the base pressure of 1 Pa, and then both temperature zones were increased up to 800 °C at a rate of 27 °C/min under a flow of 300 sccm Ar. After that, both Ga source and substrate were simultaneously delivered to the center of their respective temperature zones. Next, under a flow of 50 sccm Ar and 10 sccm O_2, the growth of β-Ga_2O_3 was maintained for 30 min under a pressure of 50 Pa. Finally, all heating was stopped and the furnace was cooled down to room temperature under a flow of 50 sccm Ar.

4.4 Characterizations

The surface morphology of h-BN was analyzed using AFM (NT-MDT solver P47) and SEM (FEI Quanta-450). Room-temperature Raman spectra were acquired with a SmartRaman confocal micro-Raman module coupled with a Horiba iHR550 spectrometer using a 532 nm laser excitation source. XPS measurements were conducted on a Thermo Scientific ESCALAB 250Xi spectrometer using monochromatic Al Kα X-ray source (1486.6 eV) with an energy resolution of 0.45 eV, and the X-ray spot size was 500 μm. The vacuum of the analysis chamber was better than 5×10^{-8} Pa. XRD θ–2θ and Φ-scan patterns of the β-Ga_2O_3/h-BN/sapphire films were obtained with a Rigaku D/MAX-2500 diffractometer using a Cu Kα (λ = 1.5406 Å) X-ray source operating at 40 kV and 150 mA. The microstructures of the h-BN/sapphire and β-Ga_2O_3/h-BN/sapphire were investigated by TEM using a Talos F200S microscope operating at 200 kV with a point to point resolution of 0.12 nm.

4.5 Computational method

First-principles DFT calculations were implemented in the Vienna *ab initio* simulation package (VASP) using the generalized-gradient approximation (GGA) for the exchange correlation functional of Perdew, Burke, and Ernzerhof (PBE). Structures were optimized with an energy and force tolerance of 10^{-5} eV and 0.01 eV/Å using the Monkhorst–Pack *k*-mesh with the size of 9 × 9 × 1. The semiempirical dispersion-corrected DFT-D3 method proposed by Grimme was employed to describe the remote vdW interaction for the calculations of c-sapphire/h-BN heterostructures. An energy cut-off of the plane-wave basis was set to be 520 eV. The vacuum region was chosen to be 20 Å. In order to minimize lattice mismatch in the sapphire/β-Ga_2O_3 heterointerface, 1 × 4 β-Ga_2O_3 ($\bar{2}01$) on the 3 × 3 sapphire (0001) was chosen. As for the sapphire/h-BN, a 3 × 3 supercell was adapted for h-BN.

Electronic Supplementary Material: Supplementary material (charge density distribution of the O-terminated c-sapphire through different interaction gaps equivalent to different numbers of h-BN layers, AFM images and XPS full-survey spectrum of the transferred polycrystalline h-BN, Raman spectra and AFM images of the h-BN layers synthesized by SSVD method, XRD patterns of the β-Ga_2O_3 films grown on the sapphire covered by a single-crystalline monolayer h-BN, the 200.1 cm^{-1} Raman mode of the β-Ga_2O_3 epilayer grown on different numbers of h-BN layers, and cross-sectional HRTEM images and full XPS survey spectrum of the β-Ga_2O_3 film grown on h-BN/sapphire substrate) is available in the online version of this article at https://doi.org/10.26599/NR.2025.94907129.

Data availability

All data needed to support the conclusions in the paper are presented in the manuscript and the Electronic Supplementary Material. Additional data related to this paper may be requested from the corresponding author upon request.

Acknowledgements

This work was financially supported by the National Natural Science Foundation of China (Nos. 62174009 and 62274151).

Declaration of competing interest

All the contributing authors report no conflict of interests in this work.

Author contribution statement

Y. M. S.: Conceptualization, data curation, investigation, formal analysis, methodology, writing – original draft. J. H. M.:

Conceptualization, methodology, formal analysis, funding acquisition, supervision, writing – review & editing. Z. C. X.: Investigation, data curation. J. D. H.: Investigation. W. K. L.: Formal analysis. J. J.: Data curation. Z. G. Y.: Formal analysis. J. X. D.: Formal analysis, X. W. Z.: Conceptualization, funding acquisition, resources, supervision, writing – review & editing. All authors contributed to discussions and finalizing the manuscript.

Use of AI statement

None.

References

[1] Pearton, S. J.; Yang, J. C.; Cary IV, P. H.; Ren, F.; Kim, J.; Tadjer, M. J.; Mastro, M. A. A review of Ga_2O_3 materials, processing, and devices. *Appl. Phys. Rev.* **2018**, *5*, 011301.

[2] Wu, C.; Wu, F. M.; Hu, H. Z.; Wang, S. L.; Liu, A. P.; Guo, D. Y. Review of self-powered solar-blind photodetectors based on Ga_2O_3. *Mater. Today Phys.* **2022**, *28*, 100883.

[3] Zhang, J. Y.; Shi, J, L.; Qi, D. C.; Chen, L.; Zhang, K. H. L. Recent progress on the electronic structure, defect, and doping properties of Ga_2O_3. *APL Mater.* **2020**, *8*, 020906.

[4] Sun, S. H.; Wang, C. L.; Alghamdi, S.; Zhou, H.; Hao, Y.; Zhang, J. C. Recent advanced ultra-wide bandgap β-Ga_2O_3 material and device technologies. *Adv. Electron. Mater.* **2024**, *10*, 2300844.

[5] Nandi, A.; Cherns, D.; Sanyal, I.; Kuball, M. Epitaxial growth of $(\bar{2}01)$ β-Ga_2O_3 on (001) diamond substrates. *Cryst. Growth Des.* **2023**, *23*, 8290–8295.

[6] Cheng, Z.; Wheeler, V. D.; Bai, T. Y.; Shi, J. J.; Tadjer, M. J.; Feygelson, T.; Hobart, K. D.; Goorsky, M. S.; Graham, S. Integration of polycrystalline Ga_2O_3 on diamond for thermal management. *Appl. Phys. Lett.* **2020**, *116*, 062105.

[7] Nepal, N.; Katzer, D. S.; Downey, B. P.; Wheeler, V. D.; Nyakiti, L. O.; Storm, D. F.; Hardy, M. T.; Freitas, J. A.; Jin, E. N.; Vaca, D. et al. Heteroepitaxial growth of β-Ga_2O_3 films on SiC via molecular beam epitaxy. *J. Vac. Sci. Technol. A* **2020**, *38*, 063406.

[8] Zhang, T.; Li, Y. F.; Zhang, Y. C.; Feng, Q.; Ning, J.; Zhang, C. F.; Zhang, J. C.; Hao, Y. Investigation of β-Ga_2O_3 thin films grown on epi-GaN/sapphire(0001) substrates by low pressure MOCVD. *J. Alloys Compd.* **2021**, *859*, 157810.

[9] Xu, W. H.; You, T. G.; Wang, Y. B.; Shen, Z. H.; Liu, K.; Zhang, L. H.; Sun, H. R.; Qian, R. J.; An, Z. H.; Mu, F. W. et al. Efficient thermal dissipation in wafer-scale heterogeneous integration of single-crystalline β-Ga_2O_3 thin film on SiC. *Fundam. Res.* **2021**, *1*, 691–696.

[10] Xu, W. H.; Zhao, T. C.; Zhang, L. H.; Liu, K.; Sun, H. R.; Qu, Z. Y.; You, T. G.; Yi, A. L.; Huang, K.; Han, G. Q. et al. Thermal transport properties of β-Ga_2O_3 thin films on Si and SiC substrates fabricated by an ion-cutting process. *ACS Appl. Electron. Mater.* **2024**, *6*, 1710–1717.

[11] Ryu, H.; Park, H.; Kim, J. H.; Ren, F.; Kim, J. Y.; Lee, G. H.; Pearton, S. J. Two-dimensional material templates for van der Waals epitaxy, remote epitaxy, and intercalation growth. *Appl. Phys. Rev.* **2022**, *9*, 031305.

[12] Park, B. I.; Kim, J.; Lu, K. Y.; Zhang, X. Y.; Lee, S.; Suh, J. M.; Kim, D. H.; Kim, H.; Kim, J. Remote epitaxy: Fundamentals, challenges, and opportunities. *Nano Lett.* **2024**, *24*, 2939–2952.

[13] Wang, X. J.; Choi, J.; Yoo, J.; Hong, Y. J. Unveiling the mechanism of remote epitaxy of crystalline semiconductors on 2D materials-coated substrates. *Nano Converg.* **2023**, *10*, 40.

[14] Roh, I.; Goh, S. H.; Meng, Y.; Kim, J. S.; Han, S.; Xu, Z. H.; Lee, H. E.; Kim, Y.; Bae, S. H. Applications of remote epitaxy and van der Waals epitaxy. *Nano Converg.* **2023**, *10*, 20.

[15] Chang, C. S.; Kim, K. S.; Park, B. I.; Choi, J.; Kim, H.; Jeong, J.; Barone, M.; Parker, N.; Lee, S.; Zhang, X. Y. et al. Remote epitaxial interaction through graphene. *Sci. Adv.* **2023**, *9*, eadj5379.

[16] Chen, Q.; Yang, K. L.; Shi, B.; Yi, X. Y.; Wang, J. X.; Li, J. M.; Liu, Z. Q. Principles for 2D-material-assisted nitrides epitaxial growth. *Adv. Mater.* **2023**, *35*, 2211075.

[17] Qiao, K.; Liu, Y. P.; Kim, C.; Molnar, R. J.; Osadchy, T.; Li, W. H.; Sun, X. C.; Li, H. S.; Myers-Ward, R. L.; Lee, D. et al. Graphene buffer layer on SiC as a release layer for high-quality freestanding semiconductor membranes. *Nano Lett.* **2021**, *21*, 4013–4020.

[18] Xu, L. Y.; Xu, Y.; Qu, Y. P.; Cao, B.; Wang, C. H.; Xu, K. Growth mechanism of exfoliable GaN by van der Waals epitaxy on wrinkled hexagonal boron nitride. *Cryst. Growth Des.* **2023**, *23*, 2196–2202.

[19] Liu, F.; Wang, T.; Gao, X.; Yang, H. Y.; Zhang, Z. H.; Guo, Y. C.; Yuan, Y.; Huang, Z.; Tang, J. L.; Sheng, B. W. et al. Determination of the preferred epitaxy for III-nitride semiconductors on wet-transferred graphene. *Sci. Adv.* **2023**, *9*, eadf8484.

[20] Lu, Y.; Krishna, S. B.; Liao, C. H.; Yang, Z. Q.; Kumar, M.; Liu, Z. Y.; Tang, X.; Xiao, N.; Hassine, M. B.; Thoroddsen, S. T. et al. Transferable Ga_2O_3 membrane for vertical and flexible electronics via one-step exfoliation. *ACS Appl. Mater. Interfaces* **2022**, *14*, 47922–47930.

[21] Min, J. H.; Li, K. H.; Kim, Y. H.; Min, J. W.; Kang, C. H.; Kim, K. H.; Lee, J. S.; Lee, K. J.; Jeong, S. M.; Lee, D. S. et al. Toward large-scale Ga_2O_3 membranes via quasi-van der Waals epitaxy on epitaxial graphene layers. *ACS Appl. Mater. Interfaces* **2021**, *13*, 13410–13418.

[22] Wang, Y. H.; Yang, Z. B.; Li, H. R.; Li, S.; Zhi, Y. S.; Yan, Z. Y.; Huang, X.; Wei, X. H.; Tang, W. H.; Wu, Z. P. Ultrasensitive flexible solar-blind photodetectors based on graphene/amorphous Ga_2O_3 van der Waals heterojunctions. *ACS Appl. Mater. Interfaces* **2020**, *12*, 47714–47720.

[23] Kim, H.; Lu, K. Y.; Liu, Y. P.; Kum, H. S.; Kim, K. S.; Qiao, K.; Bae, S. H.; Lee, S.; Ji, Y. J.; Kim, K. H. et al. Impact of 2D–3D heterointerface on remote epitaxial interaction through graphene. *ACS Nano* **2021**, *15*, 10587–10596.

[24] Han, X.; Yu, J. D.; Li, Z. H.; Wang, X.; Hao, Z. B.; Luo, Y.; Sun, C. Z.; Han, Y. J.; Xiong, B.; Wang, J. et al. Remote epitaxy and exfoliation of GaN via graphene. *ACS Appl. Electron. Mater.* **2022**, *4*, 5326–5332.

[25] Li, L. H.; Chen, Y. Atomically thin boron nitride: Unique properties and applications. *Adv. Funct. Mater.* **2016**, *26*, 2594–2608.

[26] Song, W. R.; Chen, Q.; Yang, K. L.; Liang, M.; Yi, X. Y.; Wang, J. X.; Li, J. M.; Liu, Z. Q. Recent advances in mechanically transferable III-nitride based on 2D buffer strategy. *Adv. Funct. Mater.* **2023**, *33*, 2209880.

[27] Sundaram, S.; Li, X.; Halfaya, Y.; Ayari, T.; Patriarche, G.; Bishop, C.; Alam, S.; Gautier, S.; Voss, P. L.; Salvestrini, J. P. et al. Large-area van der Waals epitaxial growth of vertical III-nitride nanodevice structures on layered boron nitride. *Adv. Mater. Interfaces* **2019**, *6*, 1900207.

[28] Wang, D. G.; Lu, Y.; Meng, J. H.; Zhang, X. W.; Yin, Z. G.; Gao, M. L.; Wang, Y.; Cheng, L. K.; You, J. B.; Zhang, J. C. Remote heteroepitaxy of atomic layered hafnium disulfide on sapphire through hexagonal boron nitride. *Nanoscale* **2019**, *11*, 9310–9318.

[29] Du, D. X.; Jung, T.; Manzo, S.; LaDuca, Z.; Zheng, X. Q.; Su, K.; Saraswat, V.; McChesney, J.; Arnold, M. S.; Kawasaki, J. K. Controlling the balance between remote, pinhole, and van der Waals epitaxy of heusler films on graphene/sapphire. *Nano Lett.* **2022**, *22*, 8647–8653.

[30] Kim, J.; Bayram, C.; Park, H.; Cheng, C. W.; Dimitrakopoulos, C.; Ott, J. A.; Reuter, K. B.; Bedell, S. W.; Sadana, D. K. Principle of direct van der Waals epitaxy of single-crystalline films on epitaxial graphene. *Nat. Commun.* **2014**, *5*, 4836.

[31] Wang, H. L.; Zhang, X. W.; Meng, J. H.; Yin, Z. G.; Liu, X.; Zhao, Y.

J.; Zhang, L. Q. Controlled growth of few-layer hexagonal boron nitride on copper foils using ion beam sputtering deposition. *Small* **2015**, *11*, 1542–1547.

[32] Chen, J. R.; Wang, G. K.; Meng, J. H.; Cheng, Y.; Yin, Z. G.; Tian, Y.; Huang, J. D.; Zhang, S. Y.; Wu, J. L.; Zhang, X. W. Low-temperature direct growth of few-layer hexagonal boron nitride on catalyst-free sapphire substrates. *ACS Appl. Mater. Interfaces* **2022**, *14*, 7004–7011.

[33] Geng, D. C.; Zhao, X. X.; Zhou, K.; Fu, W.; Xu, Z. P.; Pennycook, S. J.; Ang, L. K.; Yang, H. Y. From self-assembly hierarchical h-BN patterns to centimeter-scale uniform monolayer h-BN film. *Adv. Mater. Interfaces* **2019**, *6*, 1801493.

[34] Shi, Y. M.; Meng, J. H.; Chen, J. R.; Li, Y. M.; Wu, R.; Wu, J. L.; Yin, Z. G.; Zhang, X. W. Epitaxial growth of β-Ga_2O_3 thin films on $SrTiO_3$ (111) and (100) substrates by chemical vapor deposition. *Appl. Surf. Sci.* **2023**, *616*, 156578.

[35] Wang, Y.; Li, J. L.; Zhang, T.; Wu, W. K.; Li, W. J.; Yao, Y. X.; Wang, Z. M.; Feng, Q.; Zhang, Y. C.; Zhang, J. C. et al. Enhancing the quality of homoepitaxial $(\bar{2}01)$ β-Ga_2O_3 thin film by MOCVD with *in situ* pulsed indium. *Appl. Phys. Lett.* **2024**, *124*, 072105.

[36] Rafique, S.; Han, L.; Tadjer, M. J.; Freitas, J. A. Jr. ; Mahadik, N. A.; Zhao, H. P. Homoepitaxial growth of β-Ga_2O_3 thin films by low pressure chemical vapor deposition. *Appl. Phys. Lett.* **2016**, *108*, 182105.

[37] Yan, S. H.; Liu, Z.; Tan, C. K.; Zhang, X. Y.; Li, S.; Shi, L.; Guo, Y. F.; Tang, W. H. Anharmonic phonon scattering study in wide bandgap semiconductor β-Ga_2O_3 by Raman spectroscopy. *Appl. Phys. Lett.* **2023**, *123*, 142202.

[38] Zhang, K.; Xu, Z. W.; Zhao, J. L.; Wang, H.; Hao, J. M.; Zhang, S. N.; Cheng, H. J.; Dong, B. Anisotropies of angle-resolved polarized Raman response identifying in low miller index β-Ga_2O_3 single crystal. *Appl. Surf. Sci.* **2022**, *581*, 152426.

[39] Hao, S. J.; Hetzl, M.; Schuster, F.; Danielewicz, K.; Bergmaier, A.; Dollinger, G.; Sai, Q. L.; Xia, C. T.; Hoffmann, T.; Wiesinger, M. et al. Growth and characterization of β-Ga_2O_3 thin films on different substrates. *J. Appl. Phys.* **2019**, *125*, 105701.

[40] Feng, B. Y.; Li, Z. C.; Cheng, F. Y.; Xu, L. L.; Liu, T.; Huang, Z. L.; Li, F. S.; Feng, J. G.; Chen, X.; Wu, Y. et al. Investigation of β-Ga_2O_3 film growth mechanism on c-plane sapphire substrate by ozone molecular beam epitaxy. *Phys. Status Solidi A* **2021**, *218*, 2000457.

[41] Lv, Y.; Ma, J.; Mi, W.; Luan, C. N.; Zhu, Z.; Xiao, H. D. Characterization of β-Ga_2O_3 thin films on sapphire (0001) using metal-organic chemical vapor deposition technique. *Vacuum* **2012**, *86*, 1850–1854.

[42] Wang, G. K.; Huang, J. D.; Zhang, S. Y.; Meng, J. H.; Chen, J. R.; Shi, Y. M.; Jiang, J.; Li, J. Z.; Cheng, Y.; Zeng, L. B. et al. Wafer-scale single crystal hexagonal boron nitride layers grown by submicron-spacing vapor deposition. *Small* **2023**, *19*, 2301086.

[43] Kubota, Y.; Watanabe, K.; Tsuda, O.; Taniguchi, T. Deep ultraviolet light-emitting hexagonal boron nitride synthesized at atmospheric pressure. *Science* **2007**, *317*, 932–934.

[44] Li, X.; Sundaram, S.; El Gmili, Y.; Ayari, T.; Puybaret, R.; Patriarche, G.; Voss, P. L.; Salvestrini, J. P.; Ougazzaden, A. Large-area two-dimensional layered hexagonal boron nitride grown on sapphire by metalorganic vapor phase epitaxy. *Cryst. Growth Des.* **2016**, *16*, 3409–3415.

[45] Rafique, S.; Han, L.; Neal, A. T.; Mou, S.; Tadjer, M. J.; French, R. H.; Zhao, H. P. Heteroepitaxy of N-type β-Ga_2O_3 thin films on sapphire substrate by low pressure chemical vapor deposition. *Appl. Phys. Lett.* **2016**, *109*, 132103.

[46] Joshi, G.; Chauhan, Y. S.; Verma, A. Temperature dependence of β-Ga_2O_3 heteroepitaxy on c-plane sapphire using low pressure chemical vapor deposition. *J. Alloys Compd.* **2021**, *883*, 160799.

[47] Li, Z. M.; Jiao, T.; Li, W. C.; Wang, Z. J.; Chang, Y. C.; Shen, R. S.; Liang, H. W.; Xia, X. C.; Zhong, G. Q.; Cheng, Y. et al. Surface chemical composition and HRTEM analysis of heteroepitaxial β-Ga_2O_3 films grown by MOCVD. *Appl. Surf. Sci.* **2024**, *652*, 159327.

[48] Yatskiv, R.; Vorochta, M.; Bašinová, N.; Dinhova, T. N.; Maixner, J.; Grym, J. Low-temperature gas sensing mechanism in β-Ga_2O_3 nanostructures revealed by near-ambient pressure XPS. *Appl. Surf. Sci.* **2024**, *663*, 160155.